Contents lists available at ScienceDirect

International Journal of Electronics and Communications (AEÜ)

journal homepage: www.elsevier.com/locate/aeue

Regular paper

High gain dual-band zeroth order omnidirectional circularly polarized antenna

Harish Adhithya Murugan [*], Sriram Kumar Damodharan

Electronics and Communication Engineering Department, National Institute of Technology, Tiruchirappalli, Tamil Nadu 620015, India

A R T I C L E   I N F O

A B S T R A C T

A dual-band omni directionally circularly polarized zeroth order resonance (ZOR) antenna is proposed in this paper. Shunt ZOR (f_{sh}) is excited by an Epsilon Negative Transmission Line (ENG TL), whereas Series ZOR (f_{se}) is excited by two Pseudo-Open Termination (P-OT) unit cells. To resonate an omnidirectional f_{sh}, ENG TL is required, while to resonate an omnidirectional f_{se}, the two P-OT unit cells require similar series capacitances. Higher vertical and horizontal components are created by applying Asymmetric Unit Cells (AUCs) concept, in order to achieve Circular Polarization (CP) and high gain. The **90°** phase is provided by the ZOR. By combining the feature of omnidirectional and CP at ZOR, omnidirectional CP is achieved at both f_{sh} and f_{se}. Since ENG TL and P-OT unit cells have two **90°** right bends in the extended stubs, f_{sh} and f_{se} resonate with Left Hand CP (LHCP). The measured ZORs occur at 4.54 GHz (f_{sh}) and 3.86 GHz (f_{se}) with fractional bandwidths of 1.55% and 1.3%, respectively. The measured peak LCHP gains of the proposed antenna at f_{sh} and f_{se} are 3.34 dBic and 3.05 dBic, respectively. In the 10-dB impedance bandwidth range, the measured average axial ratio is less than 3-dB.

© 2020 Elsevier GmbH. All rights reserved.

1. Introduction

One of the most important features of the antenna design is multi-band, because a multi-band antenna can encompass wide range of applications. At the same time, achieving Circular Polarization (CP) for all the bands makes the orientation of the antenna completely independent of the transmission and reception of the signal. In most of the CP antennas, the resulting CP is always directional, which limits the antenna performance only in specific directions. This can be overcome by designing the multi-band antenna which is omni directionally CP. Zeroth Order Resonance (ZOR) is a unique frequency excited by the equivalent impedances or admittance of an Epsilon Negative Transmission Line (ENG TL) [1,2]. The equivalent impedances and admittances can be found using the formulas from [3,4]. The unit cells can also be subjected for parametric extraction using the simulated two port Z parameters [5].

Researchers have attempted to resonate ZOR using microstrip transmission line from [6–9]. In one of the attempts, a hybrid resonance is obtained using the combined excitation of Shunt ZOR (f_{sh}) and first order resonance (f_1), is reported in [6]. A vertical and a horizontal polarized f_{sh} is excited using two different ZOR antennas is designed in [7]. A complementary split ring resonator and a dual-arm spiral structure is used to resonate f_{sh} in the antenna designs of [8] and [9], respectively. Though the antenna designs from [6–9] resonate f_{sh} with low size, the excited f_{sh} has very low gain and it is linearly polarized. Researchers have also attempted to resonate a wideband f_{sh} by introducing asymmetry in the Co-Planar Waveguide (CPW) structures in [10–13]. These asymmetrical CPW structures resonate a wideband f_{sh} but suffers from very low gain and linear polarization. In some attempts [14,15], the excited f_{sh} has high gain. To achieve high gain for the excited f_{sh}, Epsilon Near Zero (ENZ) and chiral metamaterials are used in [14 and 15], respectively. But many number of unit cells are required to achieve a higher gain in [14,15] which is a disadvantage, as the size of the antenna large. In one of the attempts [16], a tri-band antenna is designed using T-shaped stub loaded ring resonator and U shaped slot, such that each resonating band is completely independent of the other. In another attempt [17], hybrid modes are excited using the substrate integrated waveguide array. But the disadvantage is, the size of the antennas in both [16] and [17] need to be higher to achieve good gains for the excited bands. Some researchers have also achieved resonating a circularly polarized f_{sh} using microstrip transmission line in [18–21]. Using circular and modified circular mushroom unit cells, a circularly polarized f_{sh} is excited in the antenna designs from

* Corresponding author.
 E-mail addresses: mhadhithya1992@gmail.com (H.A. Murugan), srk@nitt.edu (S.K. Damodharan).

[18–21]. The main disadvantage is that the excitation of multi-band ZORs will be difficult when the unit cell is circular or modified circular in shape. Moreover, the gain of the antennas from [18–21] is also very low because of the low ground dimensions. In one of the previous attempts, a dual-band ZOR which resonates f_{sh} and Series ZOR (f_{se}) using a Pseudo-Open Termination (P-OT) unit cell [22]. But it suffers from low gain, high cross polarization component for f_{se} and it requires matching elements.

Some of the researchers have also worked in exciting a circularly polarized f_{sh} using microstrip and co-planar waveguide to have high impedance bandwidth in [23–25]. But the disadvantage of the antenna designs from [23–25] is that, those designs resonates only one circularly polarized f_{sh}. Moreover, the antenna designs of [23] and [24] have low simulated efficiency at the excited f_{sh}. The high bandwidth of [24] and [25] is because these antenna designs excite both f_{sh} and f_1 at the same time. So the determination of the actual bandwidth of a ZOR is quite difficult. Moreover, the gain of the antenna designs of [23] and [25] are low.

In our previous works [26,27], a triple-band ZOR antenna is designed which resonates linearly polarized f_{sh}, f_{se} and Series ZOR1 (f_{se1}). Three ZORs are designed using two different series capacitances of the P-OT unit cells. Also in [27], a dual-band ZOR antenna is designed which resonates two linearly polarized f_{sh} and f_{se} using similar series capacitances of the P-OT unit cells. The limitations of the antennas in [26] and [27] are low gain, linear polarization for the excited ZORs and huge size. In [28], which is also our previous work, a single-band omnidirectional ZOR CP antenna is designed using the concept of Asymmetric Unit Cells (AUCs). But the drawback is the excited f_{sh} has very low gain and low fractional bandwidth. In our previous work [29], a dual-band ZOR antenna is designed such that it resonates circularly polarized f_{sh} and f_{se}, by applying the concept of AUCs. The drawbacks of [29] are very low gain, the radiation pattern of f_{se} is directional, and the physical size of the antenna is larger because of huge unused space in the right side of the antenna. The concept of AUCs is explained in detail in both [28] and [29].

When a multi-band antenna resonates with the properties of ZOR and CP, the resulting antenna has the advantage of operating in multiple frequencies, reduced size and independent of the antenna orientation. If such antennas also have the property of omnidirectional radiation, then the resulting antenna will also be direction independent.

A dual-band ZOR omnidirectional circularly polarized antenna is designed in this paper. The above antenna is proposed for the condition in which $f_{sh} > f_{se}$ ($\omega_{sh} > \omega_{se}$). For resonating f_{sh}, ENG TL is used, while for resonating f_{se} alone, two P-OT unit cells of similar series capacitances are used. Circular Polarization is achieved by the application of AUCs concept. But at the same time it is found that application of AUCs can also result in increased gain at the resonating ZOR. Both CP and high gain will be verified in this paper in detail in Sections 4 and 5. The modified rectangular mushroom unit cell is employed as ENG TL and P-OT unit cells. The omnidirectional CP is achieved because of the bending of the extended stubs in each unit cells and number of unit cells. Each unit cell has two 90° bends which makes a total of 180° otation. When two such unit cells of 180° rotation resonates a ZOR, a 360° rotation is created, which makes the radiation pattern to be omnidirectional. There are two 90° right bends in each unit cell and so the resulting ZOR will have a radiation pattern which is omnidirectional LHCP. For the verification of the ZOR, electric field plot is used, while for the verification of CP, surface current distribution is used. Matching elements are avoided by employing co-axial feed. To design, simulate and plot the various parameters of the proposed antenna, High Frequency Structure Simulator (HFSS) and Advanced Design System (ADS) are used.

The modified rectangular mushroom unit cell proposed by us in [29] is used in this design of dual-band omnidirectional ZOR CP antenna. There are two main advantages of using the modified rectangular mushroom unit cell, which are high gain and proper matching. The former is achieved by the displacement of the shorting pins of the unit cell far away from the center position. Higher the displacement, higher is the gain achieved. This can be achieved only by a rectangular shaped unit cell, because of its longer length compared to other shaped unit cells. The latter is achieved by the appropriate positioning of the P-OT unit cells and the shorting pins of the unit cells. When the modified rectangular mushroom unit cells are used, there will be a huge space around the ENG TL for the placement of the P-OT unit cells. This space will be highly limited if unit cells of others shapes like circle, square, hexagon etc. are used. This limited space will directly influence the matching, hence only rectangular shaped unit cells are preferred. Based on the above mentioned advantages, the modified rectangular mushroom unit cell is used in the design of the proposed antenna in this paper.

2. Modified rectangular mushroom unit cell and dual-band ZOR

Fig. 1(a) and (b) depict the proposed modified rectangular mushroom unit cell and its equivalent circuit, respectively.

A dispersion relation is derived using the circuit parameters in Fig. 1(b) and is presented in [1,2] which is

$$\beta(\omega) = \sqrt{\left(\left(\frac{\omega}{\omega_R}\right)^2 + \left(\frac{\omega_L}{\omega}\right)^2 - K\omega_L{}^2\right)} \tag{1}$$

where $\omega_R = \frac{1}{\sqrt{L_R C_R}}$, $\omega_L = \frac{1}{\sqrt{L_L C_L}}$, and $K = L_L C_R + C_L L_R$.

Using the formulas from [3] and [4], the circuit parameters are calculated by substituting the dimensional values of the proposed unit cell in those formulas. After using the formulas, the calculated values of the circuit parameters of the proposed unit cell are $C_R = 1.45$ pF, $C_L = 0.144$ pF, $L_R = 9.9$ nH, $L_L = 0.89$ nH [24]. These calculated circuit parameters are then substituted in $f_{sh}(\text{ShuntZOR}) = \frac{1}{2\pi\sqrt{L_L C_R}}$ and $f_{se}(\text{SeriesZOR}) = \frac{1}{2\pi\sqrt{L_R C_L}}$, which gives $f_{sh} = 4.41$ GHz and $f_{se} = 4.22$ GHz. The above calculated ZORs satisfy the condition $f_{sh} > f_{se}$, with which the antenna is designed.

From [22], it is very clear that, for resonating a f_{se}, a P-OT unit cell-1 should be included in the existing ENG TL. To maintain the excitation of f_{sh}, the shunt admittances of P-OT unit cell-1 and ENG TL must be similar. At the same time, to excite f_{se}, the P-OT unit cell-1 must have a series capacitance (C_S). The equation of C_S is derived in [22] and is given as follows,

$$C_{S1} = C_R \left\{\left(\frac{N}{N+1}\right)\left[\left(\frac{\omega_{sh}}{\omega_{se}}\right)^2 - 1\right]\right\} \tag{2}$$

where N = Number of Unit Cells in ENG TL, $\omega_{sh} = \frac{1}{\sqrt{L_L C_R}}$, $\omega_{se} = \frac{1}{\sqrt{L_R C_L}}$

Also from [27], it is very clear that another P-OT unit cell-2 should be included to the existing P-OT unit cell-1 and ENG TL to excite f_{se1}. This added P-OT unit cell-2 must also maintain the excitation of f_{sh}, hence the shunt admittances of P-OT unit cell-2, P-OT unit cell-1 and ENG TL must be similar. At the same time, to excite f_{se1}, the P-OT unit cell-2 must have a series capacitance (C_{S1}). This setup ultimately results in resonating two series ZORs (f_{se} and f_{se1}). Since in this proposed work, the main objective is to achieve omnidirectional radiation pattern, a condition is applied which is $C_S = C_{S1}$. When the series capacitances of both the P-OT unit cells become identical, the series capacitances resonate only one series ZOR or f_{se}. Fig. 2 shows the final circuit model after including the P-OT unit cell-2. The input susceptance

L	5 mm
W	10 mm
R	0.5 mm
p	10.4 mm
L_1	1 mm
L_2	5 mm
L_3	5 mm
W_1	0.5 mm
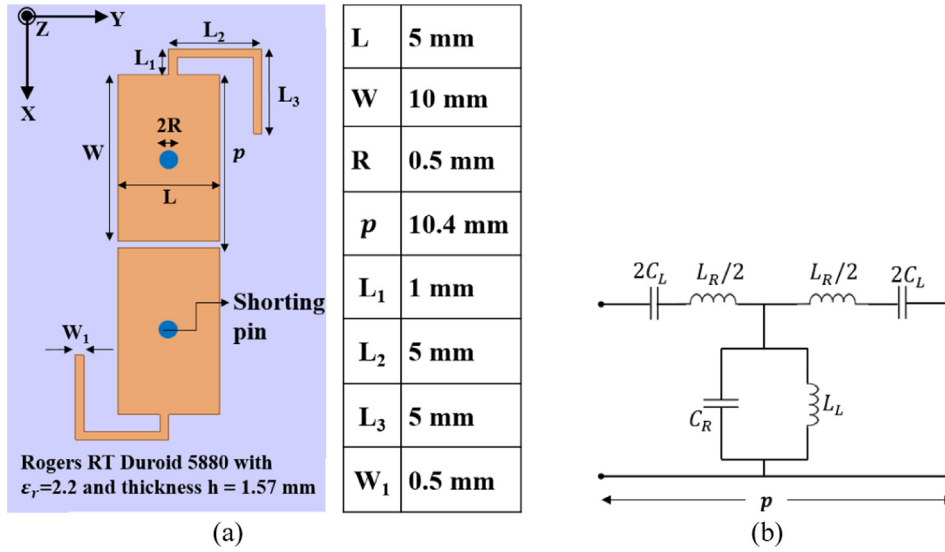
Fig. 1. (a) Modified Rectangular Mushroom Unit Cell and (b) Equivalent Circuit Model with C_L (series capacitance) and C_R (shunt capacitance), L_L (shunt inductance), L_R (series inductance).
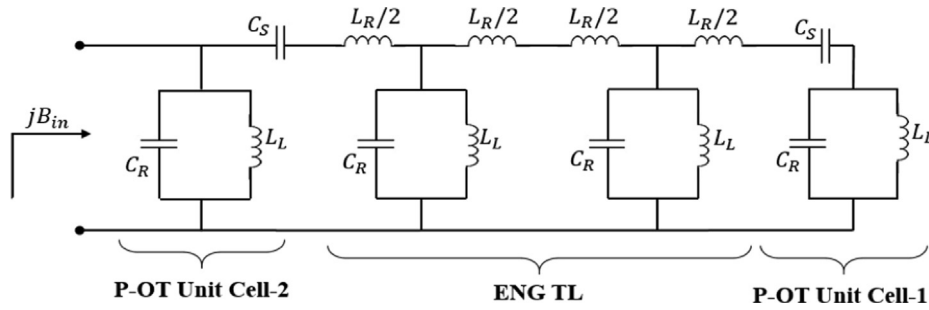
Fig. 2. Final Circuit Model of the Dual-Band ZOR.

(jB_{in}) of the equivalent circuit is obtained from [27] and is derived as follows,

$$jB_{in} = Nj\omega C_R + \frac{N}{j\omega L_L} + \frac{1}{\frac{1}{j\omega C_S} + \frac{1}{j\omega C_R + \frac{1}{j\omega L_L}}} + \frac{1}{\frac{1}{j\omega C_S} + \frac{1}{j\omega C_R + \frac{1}{j\omega L_L}}} \quad (3)$$

Now set $B_{in} = 0$, so that resonances occurs at $\omega = \omega_{se}$ and calculating for C_S, which gives,

$$jB_{in} = Nj\omega C_R + \frac{N}{j\omega L_L} + \frac{2}{\frac{1}{j\omega C_S} + \frac{1}{j\omega C_R + \frac{1}{j\omega L_L}}} \quad (4)$$

$$C_S = C_R \left\{ \left(\frac{N}{N+2}\right) \left[\left(\frac{\omega_{sh}}{\omega_{se}}\right)^2 - 1\right] \right\} \quad (5)$$

From (5) it is very clear that, change in the value of C_S affects the resonant frequency of f_{se}. Substituting the circuit parameter values $C_R = 1.45$ pF, $C_L = 0.144$ pF, $L_R = 9.9$ nH, $L_L = 0.89$ nH, N = 2, $f_{se} = 4.22$ GHz and $f_{sh} = 4.41$ GHz in (5) gives the value of capacitance $C_S = 0.07$ pF. When this series capacitance is realized using the distributed elements (or gap), the gap between P-OT unit cells and ENG TL will be large, which results in improper matching. To avoid this, f_{se} is chosen as 4.1 GHz. This chosen f_{se} must be verified for zeroth order property and it is carried out at the end of this section. When the above circuit parameters, N = 2, $f_{se} = 4.1$ GHz and

$f_{sh} = 4.41$ GHz are substituted in (5), the value of series capacitance C_S is 0.12 pF. To verify the value of series capacitance, input impedance needs to be found. This can be done by substituting the calculated circuit parameter values in Fig. 2. Using ADS, the input impedance plot is obtained which is shown in Fig. 3(a). From Fig. 3(a), it is depicted that two peaks in real value of input impedance is achieved at 4.42 GHz and 4.11 GHz which corresponds to f_{sh} and f_{se}, respectively. This shows that the peaks in the real values of input impedance is obtained because of the open termination, which validates the usefulness of the equation (5).

To verify the calculated circuit parameters with the simulation, a parametric extraction is carried out for the proposed unit cell using the simulated two port Z parameters [5]. This parametric extraction was not carried out for the unit cell proposed in the previous works. So it is done in this paper for better understanding of the proposed unit cell. After parametric extraction, the values of the extracted circuit parameters are $L_L = 0.86$ nH, $C_L = 0.143$ pF, $L_R = 9.7$ nH, and $C_R = 1.41$ pF. The comparison of both the calculated (circuit model) and the extracted (HFSS) circuit parameters using the dispersion relation in (1) is shown in Fig. 3(b). In Fig. 3 (b), the value of β at f_{sh} is very close to 0° ($\beta = 0.02°$). The value of β at f_{se} is 0.09°, which is also very close to 0°. This confirms that the chosen f_{se} which is 4.1 GHz has zeroth order property. Moreover, the value of β at f_{sh} and f_{se} is almost the same for both HFSS and circuit model. When comparing Fig. 3(a) and 3(b), it confirms

(a)   (b)
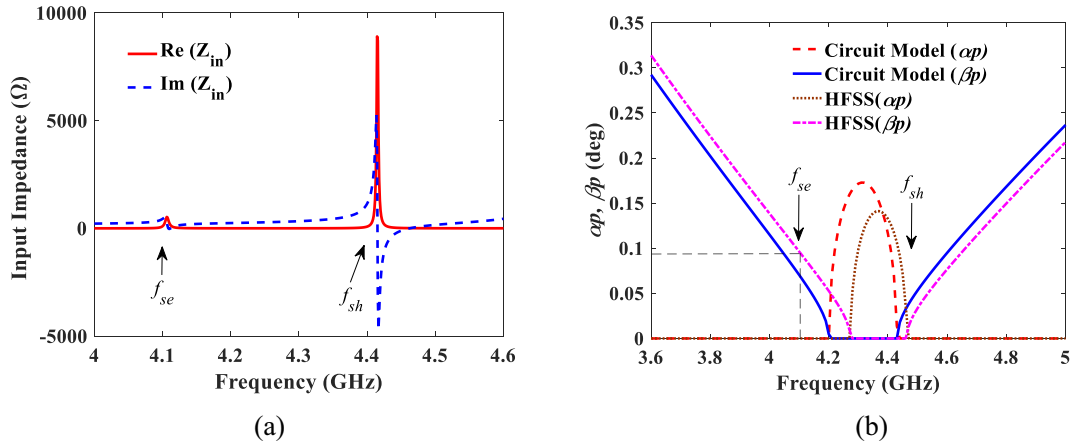
Fig. 3. Plot of the input impedance of the proposed dual-band ZOR and (b) Dispersion diagram of the proposed unit cell.

that the peak of the real value of the input impedance is achieved at the frequencies where the value of β is minimum. This confirms that both f_{sh} and f_{se} follows zeroth order property.

The concept of AUCs was explained for the proposed unit cell in [28]. Application of AUCs creates high values for both the vertical (co-polarization) and the horizontal (cross polarization) component, so that CP can be achieved for the proposed unit cell. In this work it is proved that the application of AUCs concept also leads to higher gain. This concept of high gain by the application of AUCs concept using the proposed unit cell is explained in detail in Section 4.

3. Application of AUCs in the design of dual-band ZOR omnidirectional CP antenna

Now for the realization of the equivalent circuit in Fig. 2, proposed unit cell is used. The series capacitance (C_S) of the P-OT unit cells are realized using a gap and its dimensional value is G = 0.3 mm. The resultant design is shown in Fig. 4(a), but this design does not excite f_{sh} and f_{se} with CP. Therefore, to achieve CP, unit cells-1, 3 and 4 have their shorting pins displaced to different position, which resulted in the proposed antenna shown in Fig. 4(b). The shorting pin in unit cells-1 and 3 are displaced by

(a)   (b)

(c)
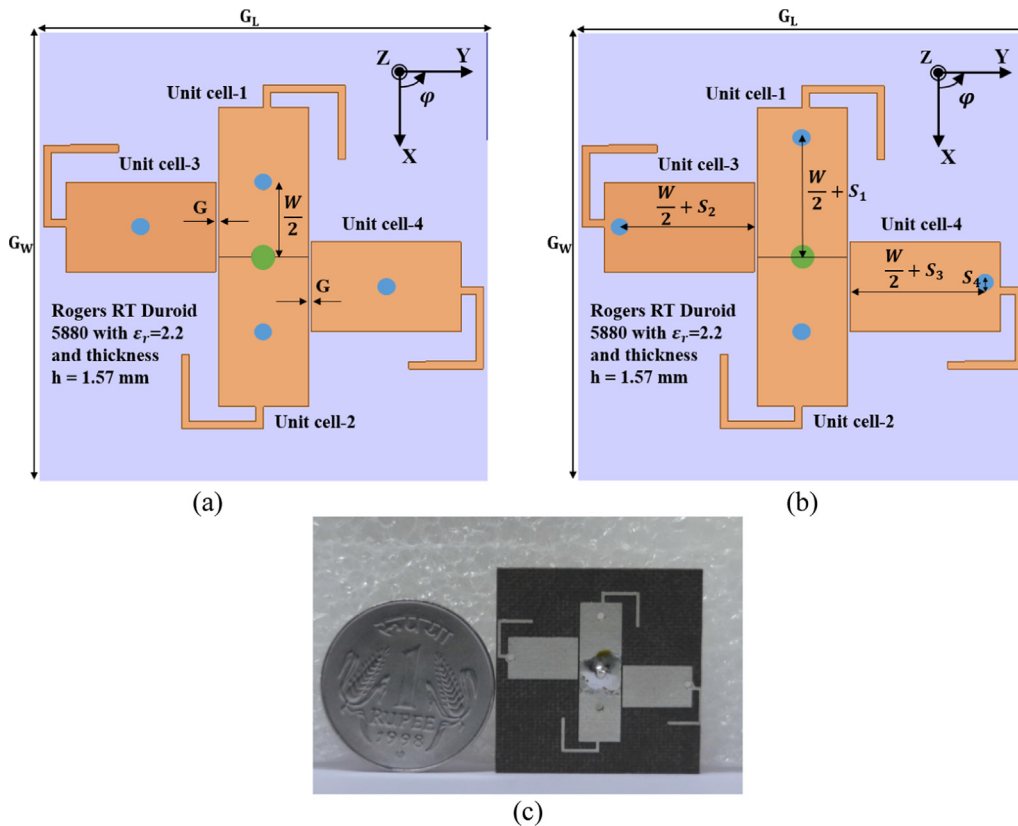
Fig. 4. (a) Dual-band ZOR antenna before applying AUCs concept, (b) Proposed antenna or Dual-band ZOR Omnidirectional CP antenna, and (c) Fabricated Prototype.

S_1 = 3 mm and S_2 = 4.5 mm, respectively. But there is a horizontal displacement and a vertical displacement of the shorting pin in unit cell-4 by S_3 = 4.5 mm and S_4 = 0.3 mm, respectively. The total dimensions of the ground is G_L = 30 mm and G_W = 30 mm. The proposed antenna is also fabricated for testing purpose, which is shown in Fig. 4(c).

To achieve both omnidirectional CP and high gain at f_{sh}, the shorting pin in unit cell-1 is displaced vertically. Similarly, in order to achieve high gain for f_{se} also, the shorting pins of unit cells-3 and 4 are shifted horizontally and far away from the center position. This setup results in high gain for f_{se} but not with CP and therefore, the shorting pin in unit cell-4 is moved vertically also, so that the horizontal component is increased and ultimately achieves CP. By doing the above vertical shift, f_{se} also achieves both high gain and omnidirectional CP.

Figs. 5 and 6 shows the field distribution plots of both f_{sh} and f_{se}. At ZOR, the unit cells resonating ZOR behaves like a capacitor [18]. This means, at ZOR, for an upward orientated electric field, there is an outward flow of surface currents from the shorting pin of the unit cells or for a downward oriented electric field, there is an inward flow of surface currents towards the shorting pin of the unit cells. Let the time period required to charge and discharge repeatedly by the unit cells be 'T'. For f_{sh}, at time t = 0, because of the negative charges on the surface of the unit cells-1 and 2, there is an upward oriented electric field over both the unit cells only, as shown in Fig. 5(a). This upward orientation confirms that the excited resonance is a ZOR and results in higher vertical component. Unit cells-3 and 4 has non uniform orientation of the electric field and therefore from Fig. 5(a), f_{sh} is excited only by unit cells-1 and 2. At time t = T/4, there is a discharge of the negative charges, which leads to the outward flow of surface currents from the shorting pins in unit cells-1 and 2 as shown in Fig. 5(b). Cancellation of surface currents do not occur because the surface current magnitude is lower in unit cell-1 compared to unit cell-2. This non cancellation of surface currents because of their unequal magnitude and opposite flow results in higher horizontal component.

At time t = T/2, because of the positive charges on the surface of the unit cells-1 and 2, a downward oriented the electric field exists as shown in Fig. 5(c). This orientation results in higher vertical component. At time t = 3 T/4, there is a discharge of the positive charges, which leads to the inward flow of surface currents towards the shorting pins in unit cells-1 and 2 as shown in Fig. 5 (d). Similar to time t = T/4, at t = 3 T/4 also complete cancellation of surface currents do not occur because of the lower surface current magnitude in unit cell-1, which results in higher value of horizontal component. From Fig. 5(a)–(d), it is very clear that at f_{sh}, the magnitudes of both the electric field and surface current vectors is lower in unit cell-1 compared to unit cell-2. This is because of the shifting of the shorting pins in unit cell-1. This setup gives higher values of both vertical and horizontal components at f_{sh}. Since there are two 90° right bends in each unit cell and the surface current also flows through those bends, the resulting CP is Left Hand CP (LHCP).

For f_{se}, at time t = 0, unit cells-3 and 4 are charged negatively because of the negative charges. So there is an upward oriented electric field vector over unit cells-3 and 4, which ultimately results in higher vertical component as shown in Fig. 6(a). At time t = T/4, there is a discharge of the negative charges, which leads to the outward flow of the surface currents from the shorting pins of unit cells-3 and 4 as shown in Fig. 6(b). Cancellation of surface currents do not occur because the surface current magnitude is lower in unit cell-4 compared to unit cell-3, ultimately resulting in higher values of horizontal component. From Fig. 6(a) and 6(b), though unit cells-1 and 2 also has an upward oriented electric field at t = 0, there is an inward flow of surface currents at t = T/4. Because of this non capacitive behavior, unit cells-1 and 2 do not resonate f_{se}. At time t = T/2, the unit cells-3 and 4 are charged positively because of the positive charges. So there is a downward oriented electric field vector over unit cells-3 and 4, which ultimately results in higher vertical component as shown in Fig. 6(c). At time t = 3 T/4, there is a discharge of the positive charges, which leads to the inward flow of surface currents towards the shorting pins of
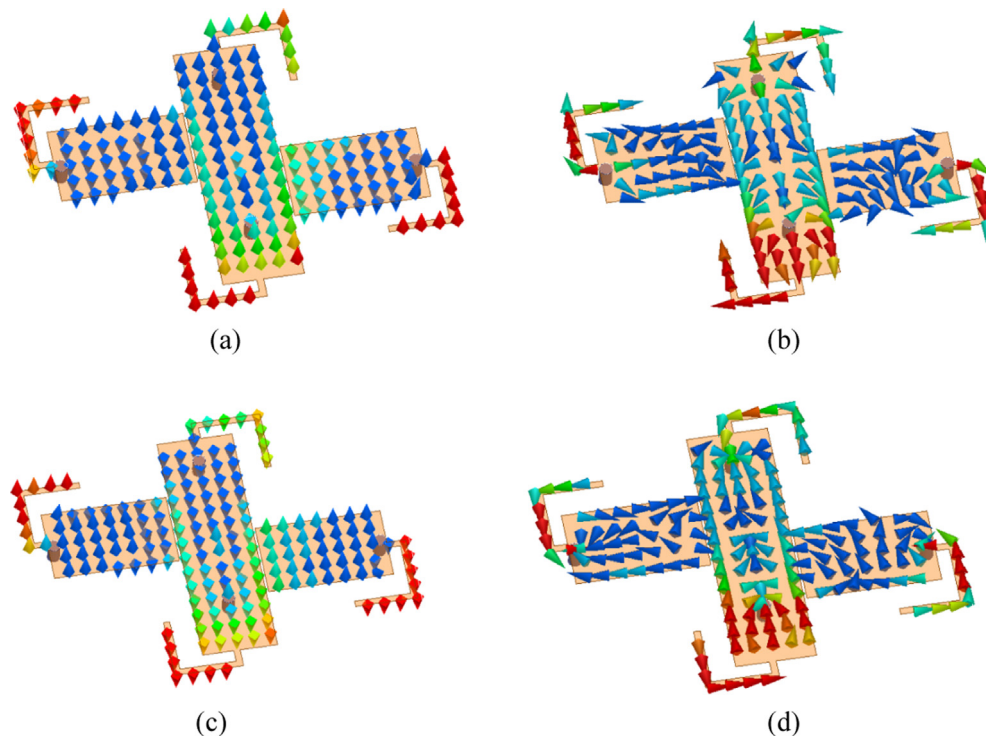
Fig. 5. Field distribution plots of the proposed antenna for f_{sh}, at time (a) t = 0, (b) t = T/4, (c) t = T/2, and (d) t = 3 T/4.
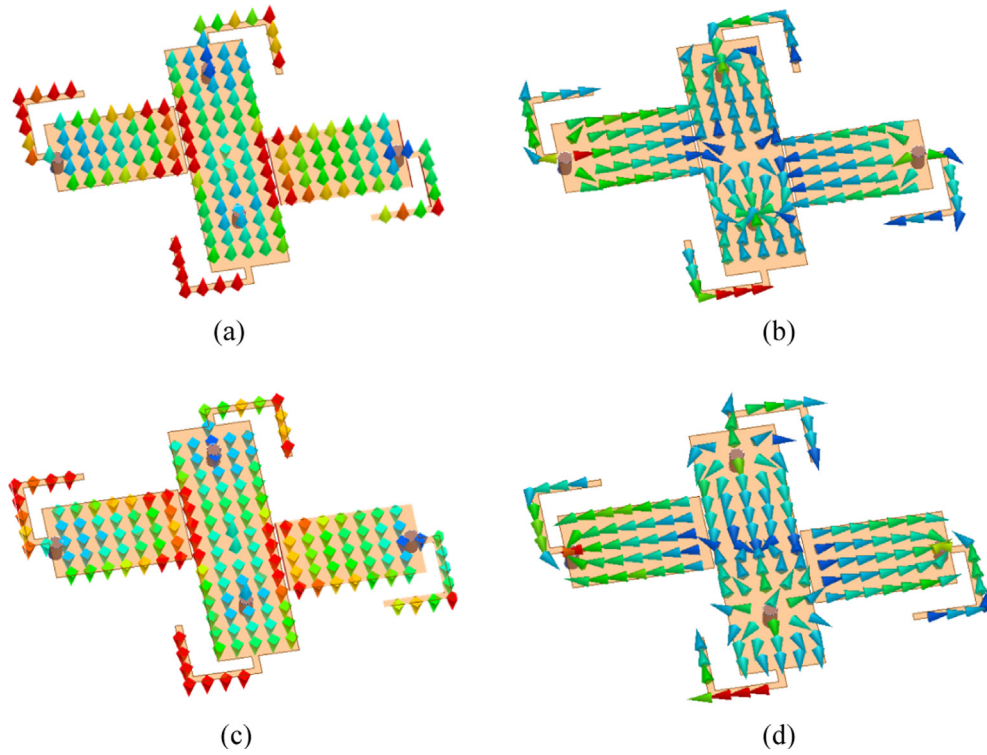
Fig. 6. Field distribution plots of the proposed antenna for f_{se}, at time (a) t = 0, (b) t = T/4, (c) t = T/2, and (d) t = 3 T/4.

unit cells-3 and 4 as shown in Fig. 6(d). Similar to t = T/4, at t = 3 T/4 also, complete cancellation of surface currents do not occur because the surface current magnitude is lower in unit cell-4, which results in higher value of horizontal component. From Fig. 6(a)–(d), unit cell-4 has lower magnitudes of both the electric field and the surface current vector compared to unit cell-3, which resulted in creating higher values of both vertical and horizontal components. Similar to f_{sh}, for f_{se} also the surface currents flow through the stubs of unit cells-3 and 4 and hence the resulting CP is LHCP for f_{se}.

4. Parametric analysis

Fig. 7 shows the parametric analysis in terms of reflection coefficient for G, R,W and L_3. These four dimensional parameters influence the resonance of f_{se} and f_{sh}. As mentioned in Section 3, varying the gap G changes the capacitance C_S and it ultimately varies f_{se} (from (5)). From [3] and [4], changing the values of R, W and L_3 directly affects the values of L_L and C_R, respectively, which in turn alters the resonance of f_{sh} and from (5), change in f_{sh} also changes the frequency of f_{se}. In Fig. 7(a), when the value of G decreases, its corresponding C_S increases and because of this increase in the value of C_S, the resonance of f_{se} decreases. Similarly when the value of G increases, the resonance of f_{se} also increases. Since changing the value of G does not affect other dimensional parameters like R, W and L_3, the resonance of f_{sh} is undisturbed in this process as shown in Fig. 7(a). In Fig. 7(b), when the value of R decreases, its corresponding value of L_L increases. From (2), when the value of L_L increases, the resonance of f_{sh} gets reduced. Similarly when the value of R increases, the resonance of f_{sh} increases as shown in Fig. 7(b). At the same time, as R decreases, there is an increase in the bandwidth of f_{se}. This is because the bandwidth of a ZOR can be found using the formula from [12] and is given as follows,

$$BW_{ZOR} = G\sqrt{\frac{L_L}{C_R}} \qquad (6)$$

where BW_{ZOR} = Bandwidth of ZOR, and G = conductance.

From Fig. 7(b), since f_{sh} does not have the value of $|S_{11}|(dB) < -10dB$ for R = 0.4 mm and R = 0.6 mm, the bandwidth analysis cannot be performed on f_{sh}. As mentioned before, by reducing the value of R, an increase in the value of L_L can be found [3]. From (6), this increase in the value of L_L will lead to a higher impedance bandwidth for f_{se}. For R = 0.4 mm, the impedance bandwidth of f_{se} is 2.2%. For R = 0.5 mm, the impedance bandwidth of f_{se} is 1.6%. For R = 0.6 mm, the impedance bandwidth of f_{se} is 1.4%. The above enhancement in bandwidth of f_{se} for different values of R is shown in Table 1. It is very clear that there is a gradual increase in the bandwidth of f_{se} when the radius of the shorting pin R is reduced gradually. Because of the in house fabrication limit, the value of R is chosen as 0.5 mm. In Fig. 7(c), when the value of W decreases, its corresponding value of C_R also decreases and from (2), this reduction in the value of C_R, increases the resonance of f_{sh}. Similarly for higher values of W, the resonance of f_{sh} reduces as shown in Fig. 7(c). In Fig. 7(d), another analysis is carried out on the value of the extended stub L_3, in which when the value of L_3 is increased, the corresponding value of C_R also increases and hence from (2) and (5), the frequencies of both f_{sh} and f_{se} are reduced considerably. At the same time, there is another advantage in increasing the value of L_3, which is the size reduction which can be seen in Fig. 7(d). A huge reduction is size can be achieved if the length of the stub L_3 is increased. But due to matching issues the optimum value of L_3 is chosen as 5 mm. If the placement of the coaxial feed and if the unit cell-3 and 4 are positioned properly, then a good matching for both f_{sh} and f_{se} can be achieved even with higher values of L_3. From Fig. 7(b), (c) and (d), change in the frequency of f_{sh} will affect the frequency of f_{se} (5), hence both the resonances are altered by varying R, W and L_3.
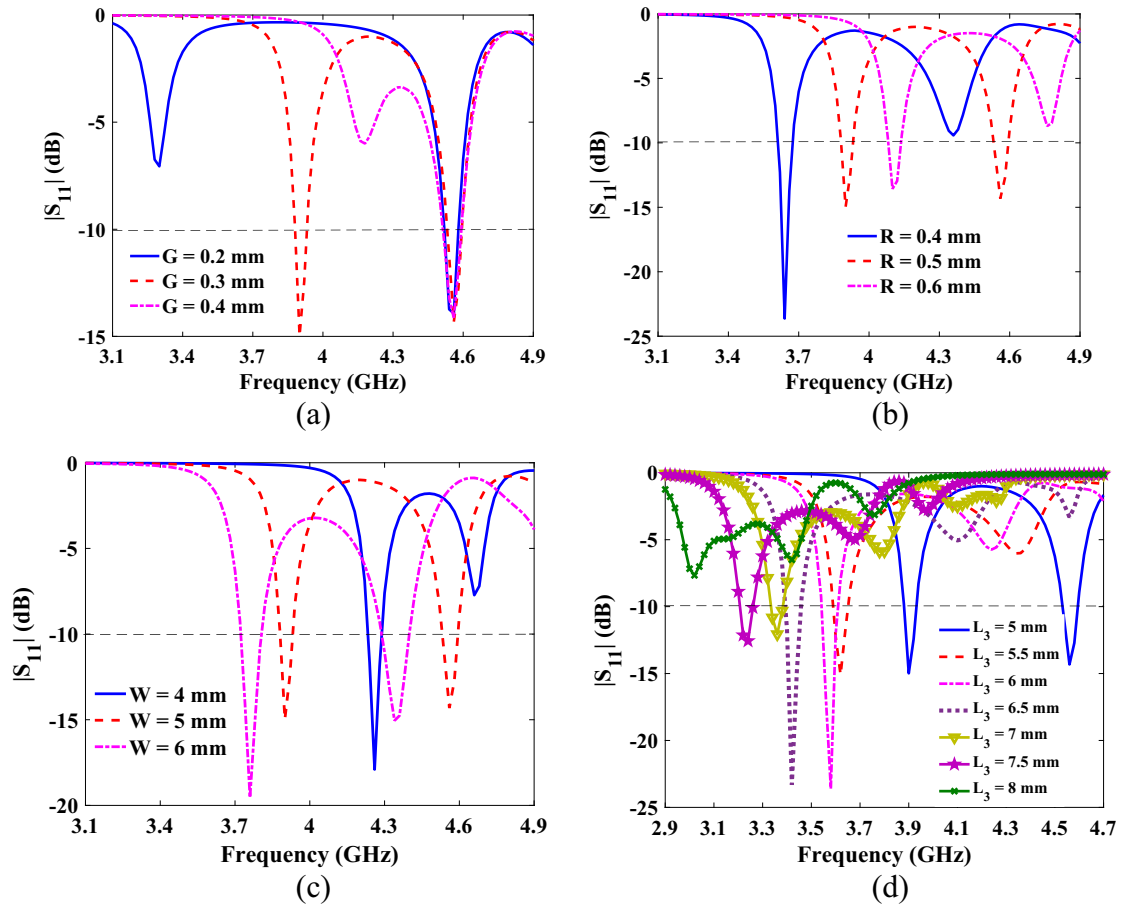
Fig. 7. Parametric analysis in reflection coefficient of the proposed antenna for different values of (a) G, (b) R (c) W and (d) L_3.

Table 1
Bandwidth enhancement of f_{se} for different values of R.

R (mm)	Simulated Impedance Bandwidth (%)
0.4	2.2
0.5	1.6
0.6	1.4

A parametric analysis is carried out for different values of S_1 to verify the increase in the LHCP gain of the proposed antenna for f_{sh} at $\varphi = 0°$ plane is shown in Fig. 8. This analysis on gain is a proof that AUCs also improves the gain of the antenna at ZOR. From Fig. 8, for lower values of S_1, the value of the peak LHCP gain is low and as the value of S_1 increases, the peak LHCP gain also increases and it achieves a maximum value for $S_1 = 3$ mm. The value of S_1 can also be increases higher, but it heavily affects the matching conditions, and therefore the value of S_1 is stopped at 3 mm. Table 2 is also provided to show the simulated peak LHCP gain for the corresponding value of S_1. The reason for the increase in the peak LHCP gain is because of the application AUCs concept. When the shorting pin of unit cell-1 is displaced, it is very obvious that high horizontal component is achieved. But at the same time, an increase in the vertical component is also observed. This leads to an almost equal values of both vertical and horizontal component. High values of both the orthogonal components leads to higher gain, whereas almost equal values of both the components leads to higher gain variation between the LHCP and the Right Hand CP (RHCP) gains, which is discussed in Section 5.

5. Results and discussion

The simulated and the measured plots of reflection coefficient for the proposed dual-band ZOR omnidirectional CP antenna is shown in Fig. 9(a). It is depicted that at 4.54 GHz (f_{sh}) and 3.86 GHz (f_{se}), the measured resonances occur. The fractional bandwidth corresponding to the measured f_{sh} and f_{se} are 1.55% and 1.3%, respectively. The measured and the simulated results are almost in correlation. The slight variation between simulation and measurement is contributed by the errors in the fabrication. The identification of the simulated ZORs after the application of AUCs is shown in the dispersion diagram in Fig. 9(b). Figs. 3(b) and 9(b) are same, but the ZORs are shifted to different frequencies in Fig. 9(b). As we know from [25] and [26], the resonance of f_{sh} is increased after applying AUCs, but because of the gaps G made by the unit cells-3 and 4 with the ENG TL, the effect gets reversed for f_{se}. This is the reason for the decrease in the resonance of f_{se}. The corresponding value of β for f_{sh} and f_{se} in Fig. 9(b) are $0.07°$ and $0.18°$, respectively. Both the values of β are close to 0°, hence the excited resonances after the application of AUCs concept obeys the zeroth order property.

From Fig. 4(b), it is obvious that the proposed antenna resonates with LHCP for both the ZORs. Fig. 9(c) and (d) corresponds to the proposed antenna's performance at f_{sh} and f_{se}, respectively in terms of the radiation pattern at $\varphi = 0°$ plane. In Fig. 9(c), for f_{sh}, in the angular range $\left[0°, 180°\right]$, there is a gain variation of more than 15 dBic between LHCP and RHCP gains. At the same time, in the angular range $\left[180°, 360°\right]$, there is a gain variation of more
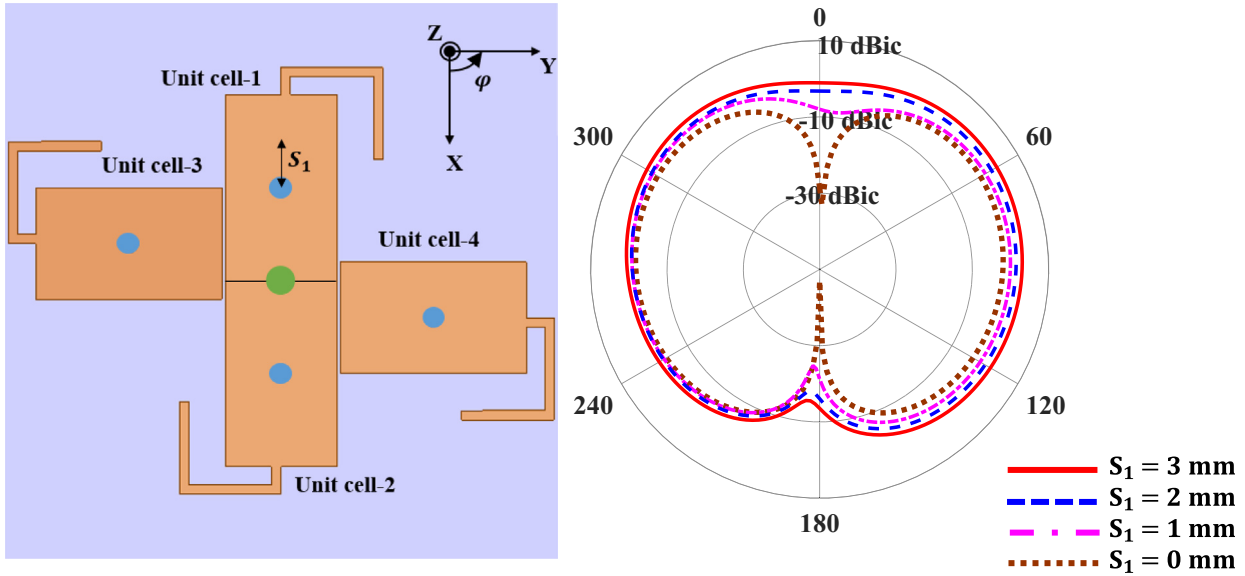
Fig. 8. Parametric analysis of the proposed antenna in terms of simulated peak LHCP gain at f_{sh} for different values of S_1. ($\varphi = 0°$ or XZ plane, Proposed antenna is shown for reference).

Table 2
Simulated Peak LHCP gain for different values of S_1.

S_1 (mm)	Peak LHCP gain (dBic)
0	−0.1
1	0.98
2	2.14
3	3.5

than 10 dBic between LHCP and RHCP gains. This clearly proves that overall, the LHCP gain is higher than RHCP gain by atleast 10 dBic, which indicates the domination of LHCP gain over the RHCP gain in the entire $\varphi = 0°$ plane, with peak measured LHCP gain of 3.34 dBic. The high gain at f_{sh} is due to the displacement of the shorting pin in unit cell-1, while the shorting pin in unit cell-2 remains at the center. The placement of unit cell-1 is at the right side when seen from $\varphi = 0°$ plane, which leads to almost equal values of both vertical and horizontal components and this is the reason for having higher variation between LCHP and RHCP gains in the angular range $\left[0°, 180°\right]$.

In Fig. 9(d), for f_{se}, in the angular range $\left[20°, 120°\right]$, $\left[180°, 200°\right]$ and $\left[220°, 360°\right]$, there is a gain variation of more than 10 dBic between LHCP and RHCP gains. In the remaining angular regions this gain variation is less than 10 dBic. The reason behind this reduced variation between LHCP and RHCP gains is the presence of the unit cells-1 and 2. In Fig. 6, though the unit cells-3 and 4 resonate f_{se} and follows the capacitive behavior, unit cells-1 and 2 has uniformly oriented electric field and non-capacitive behavior, which leads to an increase in the RHCP gains. Therefore, in the angular regions $\left[0°, 20°\right]$, $\left[120°, 180°\right]$ and $\left[200°, 220°\right]$ the variation between the LHCP and RHCP gain is minimum. But these angular regions mostly correspond to the top and bottom of the $\varphi = 0°$ plane where the value of LHCP and RHCP gains are very low. The peak measured LCHP gain at f_{se} is 3.05 dBic. Due to the small vertical displacement of the shorting pin in unit cell-4 (located at the left side when seen from $\varphi = 0°$ plane), the peak LHCP

gain occur in the angular region $\left[220°, 360°\right]$ as shown in Fig. 9(d). The LHCP gain of f_{se} is also higher because of the higher displacement of the shorting pins of unit cells-3 and 4.

The plot of the proposed antenna in terms of average axial ratio is shown in Fig. 9(e). It is very clear from Fig. 9(e), that within the axial ratio bandwidth of 2.84% for which the center frequency is at 3.87 GHz, the 10-dB impedance bandwidth of f_{se} occurs. At the same time, within the axial ratio bandwidth of 3.13% for which the center frequency is at 4.54 GHz, the 10-dB impedance bandwidth of f_{sh} occurs. So from the above points it is verified that the 10-dB impedance bandwidth occurs within the 3-dB average axial ratio bandwidth. This proves that the proposed antenna exhibits very good CP property.

In terms of the ZOR, number of unit cells, impedance bandwidth, gain, polarization, axial ratio bandwidth, simulated radiation efficiency, area and size, a comparison is shown in Table 3 between the proposed antenna and the existing ZOR designs. The antenna designs from [18–21] resonates f_{sh} with omnidirectional CP and with very low gain. But the proposed antenna resonates f_{sh} and f_{se} with omnidirectional CP, with higher gains and the number of unit cells required is also similar to [18–21]. Moreover, the antenna designs in [18,19] has very low efficiency compared to the proposed antenna. The antenna designs in [18,19] has low size but the proposed antenna occupies very less physical area and has better fractional bandwidth compared to [18,19]. The antenna designs in [20,21] has high impedance bandwidth, but the proposed antenna occupies less physical area and has low size and compared to [20,21].

The antenna designs [23,25] excites only a circularly polarized f_{sh}, while the proposed antenna excites omnidirectional circularly polarized f_{sh} and f_{se}. Though the antenna designs in [23] and [25] have better fractional impedance bandwidth, axial ratio bandwidth, the gain of these antennas are fairly lower compared to the proposed antenna at f_{sh} and f_{se}. The high bandwidth of [25] is, because the 10-dB impedance bandwidth covers both f_{sh} and f_1. So the impedance bandwidth of f_{sh} alone is impossible to find. The physical area and the size of the antenna designs in the proposed one and in [23,25] are almost similar, but at the same time, the size of the proposed antenna can be further reduced by increasing the length of the stub L_3. The radiation efficiency of the pro-
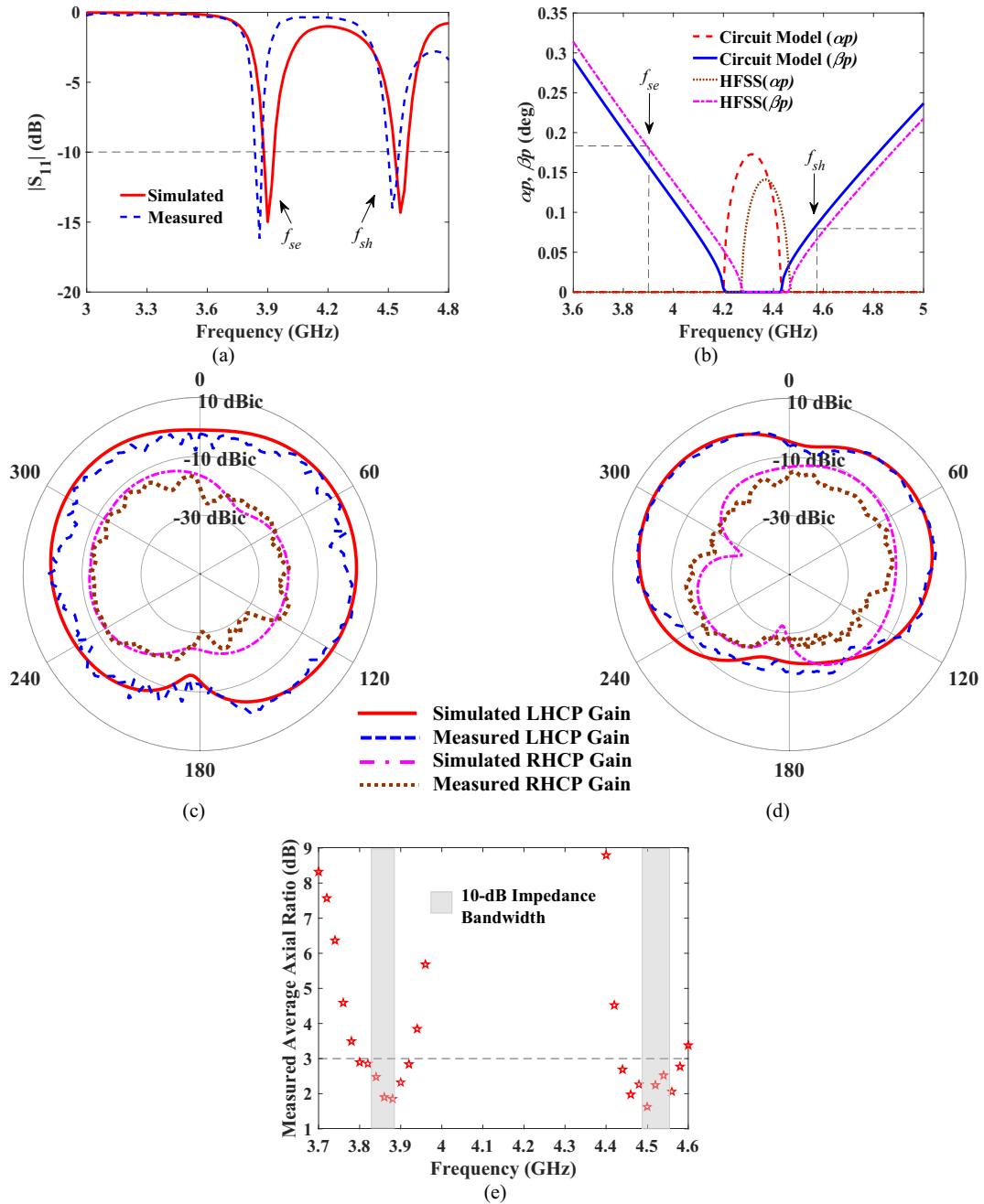
Fig. 9. (a) Plot of reflection coefficient of the proposed antenna, (b) Dispersion Diargam, *Radiation pattern of the proposed antenna at (c)* f_{sh}*, (d)* f_{se} *in XZ-plane or* $\varphi = 0^\circ$ *plane and (e) Measured average axial ratio vs frequency of the proposed antenna.*

posed antenna at f_{sh} and f_{se} is similar to [25], but much higher than the antenna in [23]

The antenna design in [24] resonates only a circularly polarized f_{sh} with high gain and high impedance bandwidth compared to the proposed antenna design. But the proposed antenna resonates circularly polarized f_{sh}, f_{se} and f_{se1}, with high axial ratio bandwidth and high efficiency. The size difference between the antenna designs of [23,24,26] and the proposed antenna may be very less, but from Fig. 7(d), the proposed antenna can be extended to have much less size by increasing the length of the extended stub L_3.

The antenna designs in [26,27] excites triple and dual-band ZOR. But the excited ZORs in [26,27] are linearly polarized with very low gain, very low fractional bandwidth and has huge size.

But the proposed antenna resonates dual-band ZOR with omni directionally circularly polarized, very high gain, has very low size and high impedance bandwidth at the excited ZORs compared to the antennas in [26,27].

The antenna design in [29] resonates a dual-band ZOR with omnidirectional CP for f_{sh} and directional CP for f_{se}, with low gain, low impedance bandwidth. But the proposed antenna resonated dual-band ZOR with omnidirectional CP for both f_{sh} and f_{se}, with higher gains and high impedance bandwidth. The antenna design in [29] and the proposed antenna occupies almost the similar physical area and has almost same size. The unused space in [29] is completely rectified in the proposed antenna which leads to the omnidirectional CP radiation for f_{se}.

Table 3
Comparison of the proposed antenna with existing methods.

Ref. No.	Name of the ZOR	Number of unit Cells	Polarization	Gain (dBic)	Impedance bandwidth (%)	Axial ratio bandwidth (%)	Radiation efficiency (%)	Physical area (mm × mm × mm)	Size of the antenna (λ_0)
[18]	f_{sh}	4	LHCP for f_{sh}	−0.4	0.539	Not given	76	56 × 56 × 3.175	0.3 × 0.3 × 0.015
[19]	f_{sh}	3	LHCP for f_{sh}	−0.24	0.49	Not given	52	33 × 33 × 3.175	0.24 × 0.24 × 0.019
[20]	f_{sh}	4	LHCP for f_{sh}	1.1	5.1	Not given	Not given	40 × 40 × 3	0.59 × 0.59 × 0.04
[21]	f_{sh}	4	LHCP for f_{sh}	1.1	4.8	Not given	Not given	40 × 40 × 3	0.63 × 0.63 × 0.05
[23]	f_{sh}	Not given	LHCP for f_{sh}	2.72	15.44	7.25	88	32 × 22 × 1.6	0.38 × 0.26 × 0.02
[24]	f_{sh}	4	LHCP for f_{sh}	4.17	10.86	2.54	75	20 × 20 × 2.6	0.24 × 0.22 × 0.05
[25]	f_{sh}	2	RHCP for f_{sh}	1.53–2.9	68.58	8.48	96.28	26 × 20 × 1.6	0.41 × 0.31 × 0.02
[26] (Triple-band ZOR)	f_{sh}, f_{se} and f_{se1}	4	Linear for f_{sh}, f_{se} and f_{se1}	2.19, 1.39 and 1.14	4.78, 0.96 and 1.5	Not given	Not given	30 × 30 × 1.57	0.69 × 0.69 × 0.03, 0.62 × 0.62 × 0.03 and 0.59 × 0.59 × 0.03
[27] (Dual-band ZOR)	f_{sh} and f_{se}	4	Linear for f_{sh} and f_{se}	2.05 and 1.4	4.1 and 1.8	Not given	Not given	30 × 30 × 1.57	0.69 × 0.69 × 0.036, and 0.61 × 0.61 × 0.031
[29]	f_{sh} and f_{se}	3	LHCP for f_{sh} and f_{se}	2.34 and 1.53	1.18 and 0.97	5.5 and 2.87	87.5 and 86.2	25 × 35 × 1.57	0.38 × 0.53 × 0.024 and 0.34 × 0.47 × 0.021
Proposed Antenna	f_{sh} and f_{se}	4	LHCP for f_{sh}, f_{se}	3.34 and 3.05	1.55 and 1.3	3.13 and 2.84	95 and 94	30 × 30 × 1.57	0.45 × 0.45 × 0.023 and 0.386 × 0.386 × 0.02

The antenna designs [26,27,29] and the proposed antenna occupies the same physical area which proves that less size and better performance can be achieved using the proposed antenna without increasing the physical area. From the above Table 3, it is clear that compared to the existing ZOR antenna designs, the proposed antenna gives a better performance.

The proposed dual-band ZOR omnidirectional antenna can be used in the C-band satellite system, especially in the receiving frequency range of the Standard C-band satellite system (f_{se}) and in the receiving frequency range of the Indian National Satellite System (INSAT) (f_{sh}). The radiation pattern of the proposed antenna as shown in Fig. 9(c) and (d) has maximum values of measured gains in the angular regions $\left[20°, 60°\right]$ and $\left[300°, 340°\right]$. The average measured LHCP gain within these angular regions is 3.25 dBic. The reason behind this is the location of India is around 23° from the equator line. This 23° has to be compensated by designing the antenna which has peak gains in the angular region around 23° and 337°. The unit cell is rectangular in shape so that the peak LHCP gain occurs in the angular regions $\left[20°, 60°\right]$ and $\left[300°, 340°\right]$. So the proposed dual-band ZOR omnidirectional antenna can be applied very well in the receiving frequency range of the INSAT system.

At the same time, from Fig. 7(d), by varying the length of the stub L_3, the ZORs can be tuned to different frequencies. By increasing the length of the stub L_3, the proposed antenna can also be used in S-band applications like WiMAX.

6. Conclusion

We have proposed a dual-band ZOR omnidirectional CP antenna in this paper. Using similar values of the series capacitances of the P-OT unit cells, an omnidirectional f_{se} is excited. AUCs concept is applied to a maximum level to achieve high gains for the excited ZORs. From the field distribution and the parametric analysis, it can be confirmed that f_{sh} and f_{se} are excited by their corresponding unit cells. The measured LHCP peak gains are 3.34 dBic and 3.05 dBic for f_{sh} and f_{se}, respectively. Also in the 10-dB impedance bandwidth range, the measured average axial ratio is less than 3-dB which proves the CP property of the proposed antenna. By carefully adjusting the value of the stub L_3, frequency tuning property for the proposed antenna can also be explored.

Declaration of Competing Interest

The authors declared that there is no conflict of interest.

References

[1] Caloz C, Itoh T. Electromagnetic metamaterials: transmission line theory and microwave applications. New York, NY, USA: Wiley IEEE Press; Dec. 2005.

[2] Dong Y, Itoh T. Miniaturized substrate integrated waveguide slot antennas based on negative order resonance. IEEE Trans Antennas Propag Dec. 2010;58 (12):3856–64.

[3] Labidi M, Dakhli N, Tabbadi O, BelHadj Tahar J, Choubani F. "Proposed Compact Antenna based on. CRLH Metamaterials", *IEEE-APS* Oct. 2013;APWC:1107–10.

[4] Bahl IJ. *Lumped elements for RF and microwave circuits*. Boston, USA: Artech House; 2003.

[5] Djeffal Z, Talleb H, Lautru D, Fouad Hanna V. Investigation on the accuracy of equivalent dielectric models for mushroom structures. IEEE-APSURI, pp. 2940-2943, 2011.

[6] Seung-Tae Ko, Jeong-Hae Lee. Hybrid zeroth-order resonance patch antenna with broad –plane beamwidth. IEEE Trans Antennas Propag 2013;61(1):19–25.

[7] Giorgio, Garavaglia, Michele, D'Amico. A compact dual-polarization ZOR antenna. Proceedings of the 9th European Microwave Integrated Circuits Conference, 2014, pp 628-631.

[8] Cheng Zhou, Guangming Wang, Yawei Wang, Binfeng Zong, Jing Ma. CPW-fed dual-band linearly and circularly polarized antenna employing novel composite right/left-handed transmission-line. IEEE Antennas Wirel Propag Lett 2013;12:1073–6.

[9] Chun-Chih Liu, Pei-Ling Chi, Yu-De Lin. Compact zeroth-order resonant antenna based on dual arm spiral configuration. IEEE Antennas Wirel Propag Lett 2014;11:318–21.

[10] Bing-Jian Niu, Quan-Yuan Feng, Pan-Lin Shu. Epsilon negative zeroth- and first-order resonant antennas with extended bandwidth and high efficiency. IEEE Trans Antennas Propag 2013;61(12):5878–84.

[11] Po-Wei Chen, Fu-Chiarng Chen. Asymmetric coplanar waveguide (ACPW) zeroth-order resonant (ZOR) antenna with high efficiency and bandwidth enhancement. IEEE Antennas Wirel Propag Lett 2012;11:527–30.

[12] Taehee Jang, Jaehyurk Choi, Sungjoon Lim. Compact coplanar waveguide (CPW)-fed zeroth-order resonant antennas with extended bandwidth and high efficiency on vialess single layer. IEEE Trans Antennas Propag 2011;59 (2):363–72.

[13] Rajasekar NV, Sriram Kumar D. Via-Less CRLH Unit Cells loaded Compact and Bandwidth-enhanced metamaterial based antennas. AEÜ-Int J Electron Commun 2017;80:48–58.

[14] George DM, Chandroth A, Ng CCH, Young PR. High-gain narrow-band slotted antenna based on ENZ SIW structure. J Phys D, Appl Phys 2018;51, Art. no. 135102.

[15] Yahong Liu, Yang Luo, Congcong Liu et al. Linear polarization to left/right-handed circular polarization conversion using ultrathin planar chiral metamaterials. Appl Phys A 2017;123(9):571.

[16] Kai Da Xu, Yong Hong Zhang, Ronald J. Spiegel, Yong Fan, William T. Joines, Qing Huo Liu. Design of a stub-loaded ring-resonator slot for antenna applications. IEEE Trans Antennas Propag 2015;63(2):517-524.

[17] Wenxun Li, Kai Da Xu, Xiaohong Tang, Yang Yang, Yanhui Liu and Qing Huo Liu. Substrate integrated waveguide cavity-backed slot array antenna using

high-order radiation modes for dual-band applications in K-band. IEEE Trans Antennas Propag 2017;65(9):4556-4565.

[18] Byung-Chul Park, Lee Jeong-Hae. Omnidirectional Circularly Polarized Antenna Utilizing Zeroth-Order Resonance of Epsilon Negative Transmission Line. IEEE Trans Antennas Propag 2011;59(7):2717–20.

[19] Park Byung-Chul, Lee Jeong-Hae. Dual-Band Omnidirectional Circularly Polarized Antenna Using Zeroth- and First-Order Modes. IEEE Antenna Wireless Propag Lett Apr. 2012;11:407–10.

[20] Cao WQ. Compact Dual Band Dual Mode Circular Patch Antenna with Broadband Unidirectional Linearly Polarized and Omnidirectional Circularly Polarized. IET Microwaves Antennas Propag 2016;10(2):223–9.

[21] Cao WQ, Wang QQ, Zhang BN, Hong W. Capacitive Probe-fed Compact dual-band dual-mode dual-polarization microstrip antenna with broadened bandwidth. IET Microwaves, Antenn Propagat 2017;11(7):1003–8.

[22] Shih-Chia-Chiu Chien-Pai Lai, Chen Shih-Yuan. Compact CRLHCPW Antennas using Novel Termination Circuits for Dual Band Operation at Zeroth-Order Series and Shunt Resonances. IEEE Trans Antennas Propag Mar. 2013;61 (3):1071–80.

[23] Mohammed Ameen and Raghvendra Kumar Chaudhary, "Metamaterial Circularly Polarized Antennas", IEEE AP Magazine, Early Access Article, 1045-9243/20©2020IEEE, 2020.

[24] Ameen M, Chaudhary RK. "Metamaterial based circularly polarized antenna employing ENG-TL with enhanced bandwidth for WLAN applications", Electron Lett, 54(20) IET; Oct. 2018, pp 1152-1154.

[25] Ghosh Kalyanbrata, Das Sushrut. A CPW-fed notched Wideband Circularly Polarized ZOR Antenna based on CRLH approach. Int J RF Microwave Comput Aided Eng 2019. https://doi.org/10.1002/mmce.21991.

[26] Harish, Adhithya, Murugan., Gudibandi, Bharath, Reddy., and Sriram, Kumar, D.: 'Triple-Band Zeroth-Order Epsilon-Negative Antenna Using Two Pseudo-Open Termination Unit Cells for C-Band Applications', IEEE Antennas Wirel Propag Lett, Vol. 18, 5, 2019.

[27] Harish, Adhithya, Murugan., Gudibandi, Bharath, Reddy., and Sriram, Kumar, D.: 'Co-axial fed Triple-band and Dual-band Zeroth Order Antennas Using Pseudo-open Termination Unit Cells for C-band Applications', AEÜ-Int J Electron Commun 2019;104:155-166.

[28] Harish, Adhithya, Murugan., Sriram, Kumar, D., Rajasekar, NV.: 'Omnidirectional Circularly Polarized Zeroth Order Antenna Using Asymmetric Unit Cells', TEQIP III Sponsored International Conference on Microwave Integrated Circuits, Photonics and Wireless Networks (IMICPW), IEEE; May 2019, pp 458 – 462.

[29] Harish, Adhithya, Murugan., Gudibandi, Bharath, Reddy., and Sriram, Kumar, D.: 'Circularly Polarized Dual-band Zeroth Order Epsilon Negative Antenna Using Asymmetric Unit Cells', International Journal of RF and Microwave Computer Aided Engineering; 2019, DOI: 10.1002/mmce.21827.

M. Harish Adhithya received B.E in Electronics and communications Engineering from Madras Institute of Technology, Anna University, Chennai, India., in 2013 and M.Tech from PSG college of Technology, Coimbatore, India in 2015. Now, he is currently working towards PhD degree in National Institute of Technology, Tiruchirappalli. His research interests are Antenna Design, Microwave Circuits, and Electromagnetic Metamaterials.

D. Sriram Kumar is currently a professor in Department of Electronics and communications engineering in National Institute of Technology, Tiruchirappalli, India. He received B.E (1991) in Electronics and Communication Engineering, Thiagarajar College of Engineering, Madurai, India and M.E (1993) with Distinction in Microwave and Optical Engineering, Alagappa Chettiar College of Engineering and Technology, Karaikudi, India and Ph.D. (2009) in Microwave Integrated Circuits – Coplanar Waveguide- Discontinuities, Periodic structures – Analysis, Antenna Applications, Bharathidasan University, Tiruchirappalli, India. He published numerous research papers in international and national journals in the areas of Microwave integrated circuits, Optical networks, Smart antennas, Carbon nanotube antennas, free space optics, Optical & Reconfigurable antennas, Flexible electronics, Photonics. And he is a Life Member of ISTE, New Delhi, India since 1995.